

# MD and multifrequency EPR studies of the dynamics of the MTSL spin-label in the activation loop of Aurora-A kinase

Maria G. Concilio,<sup>1a</sup> Alistair J. Fielding,<sup>2a</sup> Richard Bayliss,<sup>b</sup> and Selena G. Burgess<sup>b</sup>

*<sup>a</sup>The Photon Science Institute and School of Chemistry, EPSRC National EPR Facility and Service, University of Manchester, Manchester, M13 9PY, United Kingdom*

*<sup>b</sup>Astbury Centre for Structural and Molecular Biology, Faculty of Biological Sciences, University of Leeds, Leeds LS2 9JT, United Kingdom*

## Abstract

Classical molecular dynamics (MD) simulations, within the AMBER program package that runs entirely on a CUDA-enabled NVIDIA graphic processing unit (GPU), were employed to study with low computational cost and good quality of the sampling the dynamics of the methane-thiosulfonate spin label (MTSL) attached to the activation loop of the Aurora-A kinase. MD provided a wealth of information about the timescale of the different motional contributions to the overall dynamics of the spin label. These data were validated by multifrequency continuous-wave electron paramagnetic resonance (EPR) measurements, that relying on the frequency dependence of the fast and slow motions of the spin probe were used to distinguish the fast internal motion of the spin label from slow protein tumbling. It was found that the activation loop oscillated between two conformational states separated by 7 Å and the average structures obtained from the MD trajectories showed the MTSL exposed to the solvent and probing the C-lobe of the protein. The theoretical 9 and 94 GHz EPR spectra were calculated using configurations representing the interactions between MTSL and water and the tyrosine residue 208 in the C-lobe; and the comparison with experimental EPR spectra revealed that fits successfully reproduced the experimental spectra in agreement with the MD results.

---

<sup>1</sup>First corresponding email address: [mariagrazia.concilio@postgrad.manchester.ac.uk](mailto:mariagrazia.concilio@postgrad.manchester.ac.uk)

<sup>2</sup>Second corresponding email address: [alistair.fielding@manchester.ac.uk](mailto:alistair.fielding@manchester.ac.uk)

## 1. Introduction

Site-directed spin labelling (SDSL) combined with electron paramagnetic resonance (EPR) spectroscopy is a very powerful technique used widely for studying the structural properties and dynamical processes of biological systems.<sup>1-2</sup> This has provided valuable information on many proteins such as T4 Lysozyme,<sup>3</sup> lipoxygenase L-1,<sup>4</sup>  $\alpha$ -synuclein,<sup>5</sup> bacteriorhodopsin,<sup>6</sup> SNARE<sup>7</sup> and NavMs.<sup>8</sup> Studies on singly labelled proteins can reveal a wealth of information on the tumbling and diffusion properties of the target by analysis of the continuous-wave (CW) EPR lineshape.<sup>9-10</sup>

In order to provide a realistic interpretation of the CW EPR spectrum of spin labelled systems, a description of the overall dynamics of the MTSL in the protein environment has to be found. Several different computational approaches to determine the conformational space and dynamics of spin label and subsequently simulate the EPR spectrum have been suggested by several groups previously. Some approaches are based on Brownian dynamics (BD), introduced by *Robinson et al.*<sup>11</sup> and *Steinhoff et al.*<sup>12</sup>, and molecular dynamics (MD) methods introduced by *Budil et al.*<sup>13</sup> and *Oganesyan*<sup>14-15</sup> to generate stochastic dynamical trajectories of the spin labels and/or to derive diffusion parameters such as the rotational diffusion tensor, diffusion tilt angles and expansion coefficients of the orienting potentials that are then incorporated in the stochastic Liouville equation (SLE) for the calculation of the EPR spectrum. Other methods for the calculation of the EPR spectra include the stochastic Markov models<sup>16-17</sup> and temperature scaling or replica exchange<sup>18-19</sup> methods, including simulated tempering (ST) and parallel tempering (PT) that have been developed to improve sampling and kinetic information. There are also integrated computational approaches (ICA) that link a quantum mechanical (QM) method rooted on density functional theory (DFT) to the stochastic Liouville equation (SLE) equation in the Fokker-Planck (FP) form. A similar approach was used to calculate the CW EPR spectra of free radicals in their environments<sup>20-22</sup> and to study the structure and dynamics of the MTSL side chain in protein systems, such as T4 lysozyme.<sup>23-24</sup> The models produced were in good agreement with experimental data with a reasonable computational cost<sup>25-27</sup> and consistent with data obtained by MD simulations.<sup>28</sup> In these approaches QM methods were used to determine EPR parameters ( $g$ - and  $A$ -tensors) and used coarse grained methods to produce a hydrodynamic model of the diffusion tensor<sup>29</sup> that are the input of the SLE equation for the calculation of the CW EPR spectra.<sup>30</sup> There are also computationally inexpensive approaches that can be used to predict the distribution of the conformations of the spin labels and distances between spin-labelled sites, such as MMM,<sup>31</sup> PRONOX<sup>32</sup> and MtsslWizard<sup>33</sup>.

In this work, we investigated the relationship between the solution state CW EPR lineshape and the dynamics of the spin labelled activation loop of Aurora-A kinase using computational methods. Aurora-A kinase is a serine/threonine protein kinase that regulates mitotic entry, centrosome maturation and bipolar spindle assembly and is overexpressed in a number of cancers including breast, colorectal, ovarian, and glioma.<sup>34-35</sup> Kinase activity is tightly regulated by conformational changes in a conserved region of the protein known as the activation loop upon phosphorylation and binding of the activator protein Targeting Protein for Xklp2.<sup>36-37</sup> The conformation of the activation loop may also be influenced by the binding of inhibitors to the active site of Aurora-A and, in the case of the potent and selective inhibitor MLN8054, the position of the activation loop main chain is moved by up to 19 Å.<sup>38</sup> The understanding of kinase structure is mostly based on protein crystallography, which is limited by the requirement to trap the molecules within a crystal lattice.<sup>39-41</sup> Therefore, studies of kinase activation, through characterisation of activation loop conformations in solution, are important to enhance the understanding of molecular processes related to diseases and to support the discovery of small molecule kinase inhibitors.

A common spin label employed to study structural and dynamic properties of biomolecules by EPR spectroscopy is MTSL (Figure 1) that is described in our previous work<sup>42</sup> and introduced into the activation loop of Aurora-A kinase at residue 288.

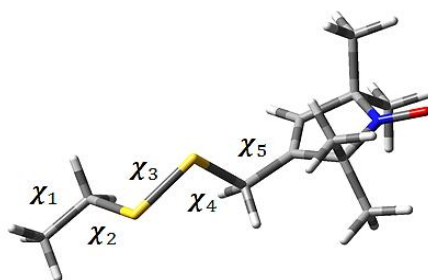


**Figure 1:** Structure of the MTSL side chain with the five dihedral angles indicated. The nitrogen and the oxygen atoms of the nitroxide group (NO) are represented in blue and red, respectively.

To allow this modification, the wild-type threonine residue was mutated to cysteine.

Here, we report a manageable workflow by using a variety of tools in order to determine all the different motional contributions to the overall dynamics of the MTSL and all the possible microenvironments probed by the spin label to obtain the fundamental information necessary to simulate the EPR spectrum. MD simulations of opportune length were performed to determine how MTSL occupies space around the point of attachment in the loop and to provide insight on the internal motion of the MTSL and its coupling with the tumbling of the protein. Subsequently, a number of configurations were chosen from MD in different environments of the protein and used for calculation of the relevant EPR parameters ( $g$ - and  $A$ -tensors) and then for the simulation of the 9 GHz and 94 GHz CW EPR spectra of the spin-labelled Aurora-A kinase.

## 2. Methods

### 2.1 Force field parameterization of the MTSL side chain and MD simulation details

The latest AMBER force field<sup>43</sup> (ff14SB), recommended for the study of protein dynamics was extended in order to perform MD simulations with AMBER 2014.<sup>44</sup> The structure of the MTSL side chain was first optimized with the B3LYP hybrid functional using the 6-31G(d) basis set. This level of theory was used as it provided accurate experimental geometries of the MTSL spin label<sup>27</sup> in previous work. Subsequently, in order to reproduce the electrostatic potential and hydrogen-bonding properties of the MTSL side chain, the atom-centred point charges were calculated with Hartree-Fock (HF) theory<sup>45-46</sup> with the 6-31G(d)<sup>47</sup> basis set, these DFT calculations were performed using Gaussian09 revision d.01.<sup>48</sup> The electrostatic potential was calculated using the restrained electrostatic potential (RESP) procedure<sup>50</sup>. The atom charges determined to extend the AMBER force field to the MTSL side chain were comparable with those reported in literature.<sup>24</sup>

MD simulations were carried out on MTSL spin labelled Aurora-A kinase, using the X-ray crystal structure of the Aurora-A kinase domain (residues 122-403 C290A C393A; PDB 4CEG<sup>50</sup> with a resolution of 2.10 Å and R-value of 0.202). The pdb file was edited in the website WHATIF<sup>51</sup> to mutate the native Threonine-288 to cysteine. Alanine substitutions were made at residues T287, C290 and C393 in order to produce a structural model similar to the experimentally studied protein. The missing crystallographic hydrogens and MTSL were added using the LEaP module AMBER. The protein was solvated using the Extended Simple Point Charge (SPC/E) water model (11896 water molecules) in a truncated octahedral box with a buffer of 12 Å between the protein atoms and the edge of the box. This water model was used as it predicts viscosities and diffusion constants closer to the experimentally observed data<sup>52</sup> and reproduces crystallographic water positions more accurately than the commonly used Transferable Intermolecular Potential 3 Point (TIP3P) water model.<sup>52-54</sup>

In order to obtain a good statistical sampling quality, multiple MD trajectories were performed<sup>55-56</sup> using multiple initial starting structures of the spin-labelled system in which the MTSL was set in different configurations with varying values of the  $\chi_1$ ,  $\chi_2$  and  $\chi_3$  dihedral angles (Table 1). These values were determined at the minima of the torsional profiles calculated in a previous work<sup>57</sup>.

**Table 1:** Initial values of the  $\chi_1$ ,  $\chi_2$  and  $\chi_3$  for trajectories from T1 to T6.

Trajectory number (n°)	$\chi_1(^{\circ})$	$\chi_2(^{\circ})$	$\chi_3(^{\circ})$
T1	-160	+80	+90
T2	+60	-120	+90
T3	-60	-160	+90
T4	-160	+80	-90
T5	+60	-120	-90
T6	-60	-160	-90

MD simulations for each trajectory were performed in three main steps: minimization, equilibration and production. Firstly, a short energy minimization was performed in two steps in order to clean the structure and to remove bad contacts using the Simulated Annealing with NMR-derived Energy Restraints (SANDER) module of AMBER. Three chloride ions were used to neutralize the net charge. In the first stage, the water molecules and counter ions were relaxed with 200 cycles of minimization. In the second step, the entire system as a whole was relaxed with 1000 cycles of minimization. Subsequently, the system was heated at constant volume for 20 ps from 10 K to 300 K with 10 kcal/mol weak restraints on the protein. This process was followed by two equilibration steps, the first was performed at constant pressure (1 atm) and temperature (300 K) for 200 ps with no restraints and the second was performed in a microcanonical (NVE) ensemble for 1 ns. The production step was performed in the NVE ensemble for at least 140 ns since transitions between rotamers occur on a time scale of ns and to ensure the full convergence of the root mean square deviation (RMSD) of the protein. All the calculations were performed using 1 fs integration time step and coordinates were collected every 2 ps, a total of 70000 frames were collected in each trajectory. The NVE ensemble was used since the interest of this work is on the dynamics of a system that would be perturbed by the use of a thermostat. This system is large enough (with 14000 atoms in total) that microcanonical and canonical ensemble are almost the same.<sup>53</sup> The dynamical long-range electrostatic interactions were treated using a particle mesh Ewald (PME) algorithm with default parameters and a 10 Å cut-off Lennard-Jones. All the MD simulation were performed using one NVidia GTX 980 GPU and with AMBER software optimized to run entirely on a CUDA enabled NVIDIA GPU using a mixed-precision SPDP (single precision, double precision) model that is comparable with the double precision model on a central processing unit (CPU).<sup>58</sup>

We would also like to highlight the advantages of running MD over QM methods and on a computer with graphic processing unit (GPU). In a previous work,<sup>57</sup> *ab initio* relaxed scans around the five dihedral angles of the MTSL were performed, five torsional profiles were computed in ~74 hours (3.1 days) on a common PC desktop (Intel CORE i7-4770 3.40 GHz CPU), considering systems composed of 23 to 41 atoms representing a short unit peptide on which the MTSL was gradually built. In contrast, one single MD trajectory of 140 ns of fully solvated spin-labelled protein system composed of 16273 atoms (4377 atoms of the protein and 11896 atoms of water) was calculated in only 81 hours (~41.05 ns/day equal to 3.4 days) using a dual Intel processor and one single NVidia GTX 980 GPU accelerator. This also helped to avoid issues related to queue limits and memory available to users in computer clusters.

## 2.4 Calculation of EPR parameters (g- and A-tensors)

The EPR parameters were calculated using the Gauge-Independent Atomic Orbital (GIAO)<sup>59</sup> method, the B3LYP<sup>60-61</sup> hybrid functional and the latest N07D basis set that has been used with success for accurate calculation of the magnetic tensors ( $\Delta g_{ii} = \pm 0.0005$ ,  $\Delta A_{ii} = \pm 1$  G) in gas phase and in solution of nitroxide radicals at a reasonable computational cost<sup>62-65</sup> and can be downloaded from the DREAMSLAB website<sup>66</sup>. The Polarizable Continuum Model (PCM) was used to describe solvation in water since the experimental EPR spectrum was measured in water<sup>67-69</sup>. All the EPR spectra were simulated using the open source *Spinach* software library, version 1.6.2782.<sup>70</sup> The slow-motion regime EPR spectra (17 ns) were simulated using the “SLE” implementation<sup>71-72</sup> based on the SLE-equation in the FP form, developed by Kubo<sup>73</sup> in the 1960’s and then adapted for EPR simulations by Freed and co-workers for the calculation of slow motion and rigid limit spectra.<sup>74-78</sup> The Fokker-Planck formalism in *Spinach* generated spatial rotations or rotational diffusion of the spin system (hence other conformations) from the starting Cartesian coordinates obtained from the selected frames. The fast-motion regime EPR spectra (2, 5 and 7 ns) were simulated using the Bloch-Redfield-Wangsness relaxation theory.<sup>79-80</sup> The static powder simulation of the 95 GHz spectrum at 150 K was performed using the powder context with the Levedev spherical grid rank 131.

## 2.5 Experimental section

The expression construct for Aurora-A 122-403 T287A, T288C, C290A, C393A was produced in earlier work for recombinant expression of the protein in *E. coli* with a N-terminal TEV cleavable His<sub>6</sub>-tag.<sup>37</sup> Expression and purification of the kinase was carried out as previously stated with the following modifications.<sup>50</sup> After TEV cleavage and affinity chromatography to remove the His<sub>6</sub>-tag and His<sub>6</sub>-tagged TEV, 5 mM DTT was added to Aurora-A containing fractions and left to incubate overnight at 4 °C to ensure C288 was in the reduced form to allow subsequent modification with MTSL. The reducing agent was removed by desalting of the protein on a HiPrep 26/10 Desalting column as per the manufacturer’s instructions (GE Healthcare) into 20 mM Tris pH 7.0, 0.2 M NaCl, 5 mM MgCl<sub>2</sub> & 10 % (v/v) glycerol (EPR buffer). 10-fold excess MTSL was added to the kinase and incubated overnight at 4 °C in order to spin label the kinase. Any remaining impurities, aggregated protein and excess MTSL were removed by size-exclusion chromatography using a HiLoad 16/600 Superdex 200 pg column as per the manufacturer’s instructions (GE Healthcare) into EPR buffer. SDS-PAGE analysis was used to identify fractions of high purity MTSL-Aurora-A 122-403 T287A, T288C, C290A, C393A which were concentrated and flash-frozen for future experiments. 50  $\mu$ M MTSL-Aurora-A 122-403 T287A, T288C, C290A, C393A was used for CW EPR studies. 9 GHz measurements were performed using a Bruker Micro EMX spectrometer at 298 K, the modulation frequency was set at 100 KHz and the microwave power at 2.0 mW. The spin labelling efficiency was equal to 86% as measured following a published procedure.<sup>81</sup> 93.778 GHz CW measurements were performed at 298 K and 150 K on a Bruker E560 spectrometer. The magnetic field was calibrated using a Mn<sup>2+</sup> power standard (0.02% MgO) and the procedure described by O. Burghaus *et al.*<sup>82</sup> Dual-scan measurements were made in order to avoid hysteresis effects and a modulation frequency of 100 KHz and low microwave power (0.004800 mW) were used to avoid distortion of the lineshape.

### 3. Results and discussion

#### 3.2 Dynamics of the MTSL spin label in the activation loop of the Aurora-A kinase protein

All the six trajectories showed the MTSL fully probing the space around the point of attachment and exploring all the regions surrounding the loop. Appropriate sampling was obtained, simulation results converged to stable RMSDs (Figure 1 ESI) after 1-2 ns (for T1, T2 and T3) or after 20 ns (for T4, T5 and T6). The most populated values of  $\chi_1$ ,  $\chi_2$ ,  $\chi_3$ ,  $\chi_4$  and  $\chi_5$  observed in the six trajectories were comparable with minima values of the torsional energy profiles obtained by QM in a previous work<sup>58</sup>. Three minima were found in the torsional profile of  $\chi_1$  corresponding to  $-160^\circ$ ,  $-60^\circ$  and  $+60^\circ$  and the same three minima were found in the plot of the occurrences (Figure 2 ESI) from which also the minima of  $\chi_2$  were confirmed and so on for  $\chi_3$ ,  $\chi_4$  and  $\chi_5$ . The plot of the transitions of the five dihedral angles (*e.g.* transitions in T1, Figure 3 ESI) over the time of the MD simulation showed slower transitions of  $\chi_1$  due to the higher energy barriers of about 6 kcal mol<sup>-1</sup> separating the conformational minima, while  $\chi_2$ ,  $\chi_4$  and  $\chi_5$  undergo faster transitions due to the lower energy barriers of 1-4 kcal mol<sup>-1</sup>. Transitions of the dihedral angle  $\chi_3$ , representing the disulphide bond of the side chain, were seen to occur very rarely, probably due to the high energy barrier of about 10-20 kcal mol<sup>-1</sup>,<sup>57</sup> they did not occur in the starting structures T2, occurred once in T3, twice in the T1, three times in T4 and T5, four times in T6. Another observed feature was the coupling between transitions of dihedral angles close to each other, *e.g.* the simultaneous transitions of all the five dihedral angles at 16.7 ns and the transitions of  $\chi_1$  and  $\chi_2$  between 23 and 55 ns. In order to identify a correlation between motions of the MTSL side chain and the activation loop, a comparison between the RMSD of the loop backbone and the evolution of the torsional profiles of dihedral angles of the MTSL was made. A coupling between transitions of the RMSD and transitions of  $\chi_1$ ,  $\chi_2$  and  $\chi_4$  was found, especially of  $\chi_4$  (Figure 4 ESI). Transitions  $\chi_3$  and  $\chi_5$  were found to be too slow and fast, respectively (Figure 3 ESI) to identify a clear correlation with the activation loop movements.

#### 3.3 Analysis of the main motional contributions in the protein systems

In order to determine the magnitude of the main motional contributions occurring in the protein system, the rotational correlation times,  $\tau_R$  related to the internal motion of the MTSL side chain and the tumbling of the protein were determined. An estimation of the internal motion of the side chain was provided analysing the transitions of  $\chi_4$ , since there are many X-ray crystallographic and spectroscopic studies of the rotameric states of the MTSL indicating that its internal dynamics arise predominantly from the dihedral angles  $\chi_4$ .<sup>29, 83</sup> The speed of the transitions were seen to be dependent on the trajectory, *e.g.* Figure a shows the transitions of  $\chi_4$  in T1 (Figure 5A ESI) and T4 (Figure 5B ESI) that occurred on timescales that went from 7 ns to 4-5 ns and between 1 to 2 ns, respectively. Similar timescales were observed in the other trajectories. Transitions of  $\chi_4$  were found to be particularly coupled with the transitions of the RMSD of loop backbone. It is possible to observe that when the RMSD was constant, *e.g.* in Figure 5A ESI from 25 to 40 ns (RMSD equal to 3.9 Å), and in Figure 5B ESI from 40 ns to 48 ns (RMSD equal to 2.1 Å) the activation loop was moving slower and there are well-defined transitions of  $\chi_4$  between two values  $180^\circ \leftrightarrow +70^\circ$  or  $180^\circ \leftrightarrow -70^\circ$ . When there were larger transitions in the RMSD, *e.g.* in Figure 5A ESI from 10 ns to 25 ns and in Figure 5B ESI from 10 to 20 ns, the activation loop was moving faster and also transitions between the three values,  $+70^\circ \leftrightarrow 180^\circ \leftrightarrow -70^\circ$ . Hence, in accordance to that was observed in Figure 5 ESI an approximation of the rotation correlation time,

$\tau_R$  of the internal motion of the MTSL can be given, fixing it between 2 to 7 ns corresponding to faster and slower transitions of  $\chi_4$ .

The rotational correlation time of the tumbling of the protein was determined using the Stokes-Einstein-Debye equation  $\tau_R = \frac{k_B T}{8\pi\eta R_h^3} = \frac{1}{6D_r}$ , where  $k_B$  is the Boltzmann constant,  $T$  is the temperature,  $\eta$  is the viscosity of the water at 298 K,  $R_h$  is the hydrodynamic radius of the protein and  $D_r$  is the rotational diffusion coefficient.  $D_r$  was calculated for the PDB:4CEG structure of Aurora-A kinase using the program HYDROPRO<sup>84</sup> and was equal to  $9.560 \times 10^6 \text{ s}^{-1}$ , the corresponding  $\tau_R$  was equal to 17 ns. Figures 2 shows a comparison between experimental and simulated 9 GHz EPR spectra of the spin-labelled Aurora-A kinase, measured

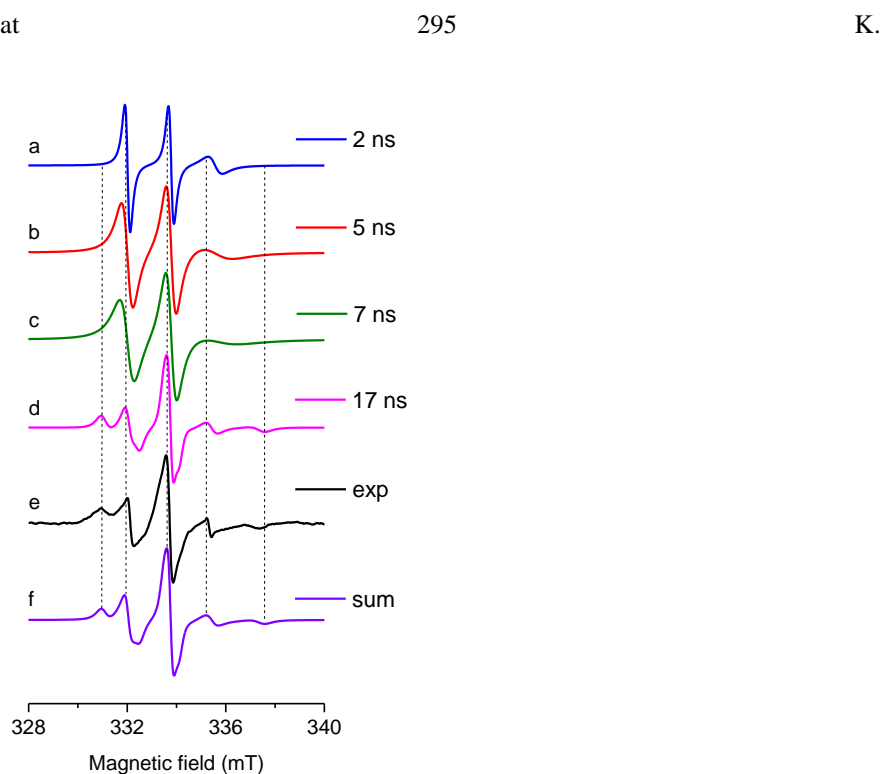


**Figure 2:** Comparison between experimental (black line) and simulated (coloured lines) 9 GHz EPR spectra at 298 K of the Aurora-A kinase using values of  $\tau_R$  equal to 2 ns, 5 ns, 7 ns and 17 ns. The simulated spectra were calculated keeping the magnetic parameters ( $g$ - and  $A$ -tensor) constant and no artificial line broadening parameters were included in the simulations.

The 9 GHz EPR spectra of MTSL spin-labelled proteins are affected by both the fast internal motion of the spin label and by slow protein tumbling,<sup>29</sup> the latter is predominant while the former is averaged out.<sup>85</sup> Therefore, the rotational correlation times from 2 to 7 ns (representing the internal motion of the MTSL) and 17 ns (representing the global tumbling of the protein) were used to simulate spectra. It was observed that simulations using  $\tau_R$  from 2 to 7 ns generated three sharp lines that broaden when  $\tau_R$  increases. These lines did not fit the full experimental EPR spectrum at 9 GHz, while the simulation with  $\tau_R = 17$  ns gave good fits to the full spectrum. However, some improvements in the fit could be obtained by summing spectra a, b and c in the same amount and add a 25% contribution of the resulting spectrum to the spectrum d to obtain spectrum f.

A similar analysis was performed at 94 GHz where fast motional processes are detected and slow motions are frozen out. The comparison between experimental and simulated 94 GHz spectra of the spin-labelled Aurora-A kinase, measured at 298 K is shown

in Figure 3.

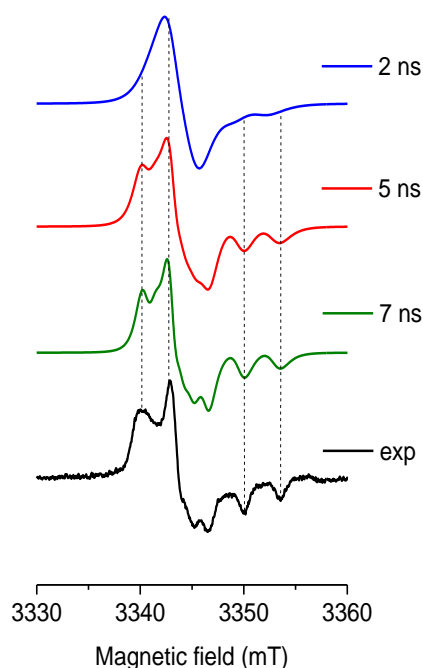


**Figure 3:** Comparison between experimental (black line) and simulated (coloured lines) 94 GHz EPR spectra at 298 K of Aurora-A kinase using values of  $\tau_R$  from 2 to 7 ns. The simulated EPR spectra were calculated keeping the magnetic parameters ( $g$ - and  $A$ -tensor) constant and no artificial line broadening parameters were included in the simulations.

As expected, motions that appeared fast at lower frequencies appear slow at higher frequencies<sup>86</sup> and good fits were obtained using  $\tau_R$  equal to either 5 ns or 7 ns, especially using 7 ns, whilst simulations with  $\tau_R$  equal to 2 ns provided too sharp resonances and poor fit to the spectrum. Bringing together the work at 9 and 94 GHz (Figure 2 and 3), it was possible to conclude that the magnitude of the internal motion of the MTSL can be approximated to 5-6 ns, an average value between 2 ns and

7

ns.

### 3.3 Analysis of the conformational states adopted by the Aurora-A kinase activation loop

In all the six MD trajectories it was observed that the activation loop oscillated between the two extreme conformational states, separated by the average distance of 7.2 Å (Figure 4) and explored many other conformational states in between them that were consistent with published X-ray crystal structures.<sup>36-37, 51</sup>

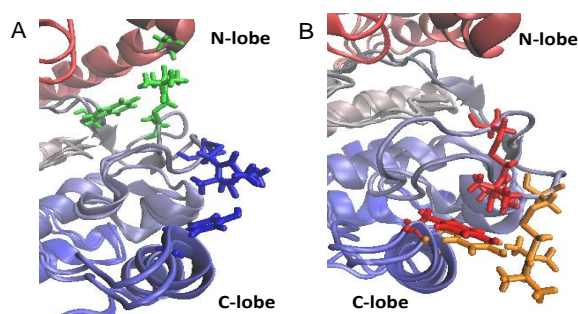


**Figure 4:** (A) Two different conformational states of the activation loop in which MTSL probed different regions; the green MTSL is probing the  $\alpha$ -helix in the N-lobe and the blue MTSL is probing the  $\alpha$ -helix in the C-lobe; (B) two different conformational states of the activation loop in which the MTSL probed the same region, the  $\alpha$ -helix in the C-lobe.



However, it was observed that due to the relatively long length of the MTSL (10 Å) and due to relatively small gap between conformational states adopted by the activation loop in the MD trajectories, the MTSL can explore both regions of the N- and C-lobes from all the possible conformations of the activation loop, indicating not a particular correlation between the regions explored by the MTSL and conformations of the activation loop (Figure 4). The distances, in the average structures obtained from the six MD trajectories, between N- and C-lobes and the activation loop were seen to be comparable to those observed in the starting X-ray crystal structure (Figure 6 ESI) and equal to 12.8 Å and 11.3 Å, respectively. However, MD revealed that the distances between the C-lobe and the activation loop are  $\sim 1\text{-}2$  Å less than the distance observed in the 4CEG X-ray crystal structure ( $\sim 13$  Å).

### 3.4 Characterization of the microenvironments probed by the MTSL spin label using multifrequency EPR spectroscopy

In order to elucidate the EPR spectrum of the Aurora-A kinase, the average structures obtained from the six trajectories were considered; in four of these structures the MTSL was exposed to the solvent and pointed to different positions in space and faraway from the N- and C-lobes, while in the remaining two, the spin label was interacted with tyrosine 208 in the  $\alpha$ -helix of the C-lobe (Figure 7 ESI). However, five different configurations were extracted from MD, representing the different microenvironments probed by MTSL in the regions of the N- and C-lobes, characterized by different polarity. The N-lobe was seen to be more hydrophobic due to the presence of amino acids, such as tryptophan and alanine, while the region of the C-lobe and the activation loop was seen to be more hydrophilic due to large exposure to solvent and to several residues of tyrosine and glutamine.

In Figure 5a, the red MTSL represents a conformation fully exposed to the solvent and interacting only with water, the blue MTSL represents an interaction with tyrosine 208 only (Figure 5b), the pink MTSL represents an interaction with both the tyrosine 208 and glutamine 209 (Figure 5c), the grey MTSL represents an interaction with the glutamine 209 only (Figure 5d) and the green MTSL represents an interaction with both alanine 46 and tryptophan 151 (Figure 5e).

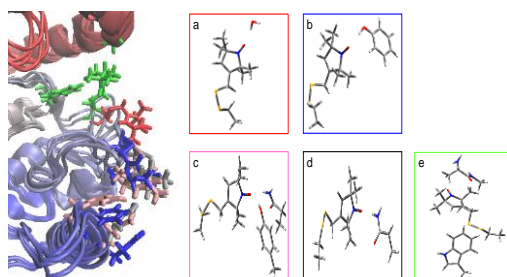


**Figure 5:** Five different frames extracted from the MD simulations showing MTSL in different configurations represented by different colours.

The EPR parameters of these structures were calculated at B3LYP/N07D level of theory using the PCM water model and all the simulations were performed considering a molecular reference frame with  $g$ - and  $A$ -tensors collinear, since all of the six trajectories showed an isotropic and uniform distribution of orientations (Figure 8 ESI), and therefore the effect of different orientations of the  $A$ - and  $g$ -tensors with respect to specific laboratory frame (aligned to the magnetic field) can be considered

lost. Figure 6 shows the comparison between experimental and theoretical 9 GHz and 94 GHz EPR spectra, measured at 298 K and 150 K, respectively.

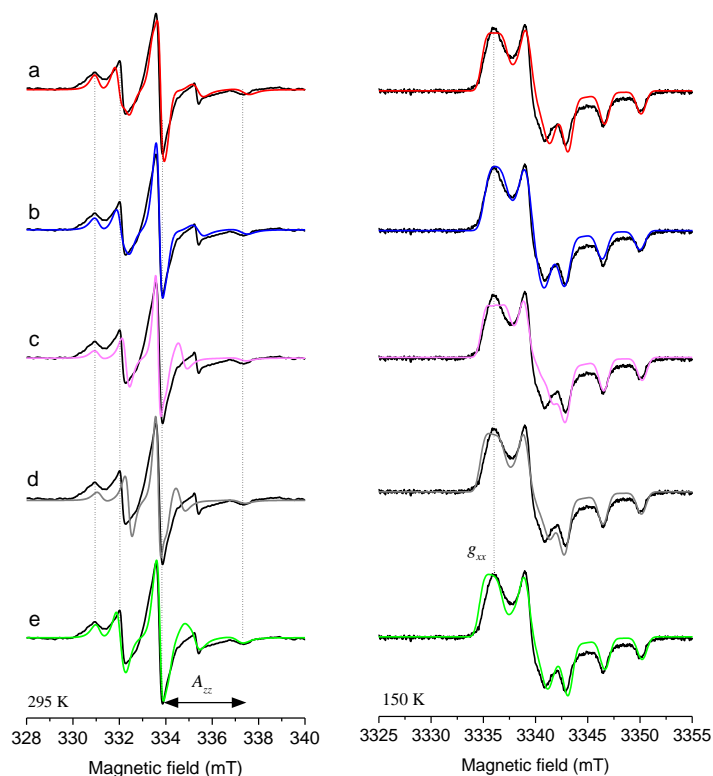


**Figure 6:** 9 GHz (left) and 94 GHz (right) EPR spectra measured at 298 K and 150 K, respectively. The black lines represent the experimental spectra and the coloured lines simulated EPR spectra using the structures shown in the insert corresponding to the structures shown in the box A. The 9 GHz EPR spectrum was simulated using a correlation time of 17 ns. The horizontal arrow represents amplitude of the  $A_{zz}$  component of the hyperfine tensor and  $g_{xx}$  is the component of the  $g$ -tensor.

The simulated EPR spectra in Figure 6 a, b and c reproduced well the experimental data, especially a and b, whilst fits between spectra c and d were in poor agreements at both 9 and 94 GHz. Similar spectra arose from other frames extracted from MD describing similar interactions and comparable poor fits were obtained also from frames describing interactions between the MTSL and amino acids, such as arginine and lysine containing the amine ( $\text{NH}_2$ ) group. Spectra c and d are characterized by smaller  $g_{yy}$  and  $A_{yy}$  (evident in both the 9 GHz and 94 GHz spectra), while simulated EPR spectrum e was characterized by larger  $A_{xx}$  (evident in the 9 GHz spectrum) and  $g_{xx}$  (evident in the 94 GHz spectrum); the EPR spectra a and b are characterized by  $A$ - and  $g$ -tensors matching the experimental spectrum. Figure 6 also showed the effect of the polarity of the different micro-environments on the  $A_{zz}$  component of the hyperfine tensor (Figure 6, 9 GHz) and on the  $g_{xx}$  component of the  $g$ -tensor (Figure 6, 94 GHz) due to the magnetic field along the  $x$ - and  $z$ -axes of the nitroxide bond (NO).<sup>87-88</sup> The 9 GHz EPR spectra are dominated by the hyperfine anisotropies and it is possible to determine the amplitude of  $A_{zz}$ , while the  $g$ -tensor is well-resolved at 94 GHz.<sup>85</sup> Structures a and b in Figure 5 are located in polar environments, structures c and d are located in a less polar environment, whilst structure e is located in a nonpolar environment. Table 1 in ESI shows the evolution of the  $A_{zz}$  component and the  $g_{xx}$  components, as expected, the  $A_{zz}$  was seen decreasing with the increase of the polarity of the environment (from a to e), while the  $g_{xx}$  was observed to increase with polarity (from a to e).

The full EPR spectrum of the Aurora-A kinase was seen to be successfully simulated using one correlation time of 17 ns, indicating a predominant contributing of the isotropic rotational tumbling of the protein at 9 GHz, as expected and considering EPR magnetic parameters of structure a and b (Figure 5). However, if the contributions of the internal motion of the MTSL and any free spin label present in the medium are considered, further improvement in the fit of the spectra a and b in Figure 6 can be obtained, since the sharp feature at 335 mT in 9 GHz experimental spectrum spectrum was better reproduced (Figure 9 ESI). If these contributions are included to the spectrum e in Figure 6, distortions were observed (Figure 9 ESI). This is in good agreement with that was observed in the MD trajectories that showed the average structures with the MTSL exposed in the solvent water (represented by the red MTSL in Figure 5) and interacting with the tyrosine 208 in the C-lobe (represented by the blue MTSL in Figure 5).

#### **4. Conclusion**

The work described here demonstrated the advantages of running MD simulations on a GPU that provided a reliable and realistic description of the conformational space of the MTSL in the full protein environment in a short time frame.

Conformational states of the MTSL obtained from MD simulations were in good agreement with those obtained from QM calculations performed previously<sup>57</sup> with the advantage that the dynamics of the full system were considered. MD revealed that the activation loop oscillated between two conformational states separated by about 7 Å and the distances between activation loop and the N- and C- lobes were seen to be consistent with those observed in the X-ray crystal structures. The experimental 9 GHz EPR spectrum of the Aurora-A kinase at 298 K was easily simulated with just one rotational correlation time of 17 ns, indicating isotropic tumbling of the protein. However, improvements in the fit were obtained considering the internal motion of the MTSL (~6 ns) and the free spin label. The agreement between simulated and experimental 9 GHz and 94 GHz EPR spectra was consistent with that observed in the average structures obtained from the MD trajectories that showed the MTSL exposed to the solvent and interacting with the tyrosine 208 in the C-lobe. A realistic picture of the MTSL in the Aurora-A kinase was provided in a relatively simple way using publically available software without over parameterizations. This detailed protocol can be easily applied to other spin and/or biological systems to test a broad applicability.

#### **5. Future work**

The correlation between the tumbling of the protein and the evolution of  $\chi_4$  revealed the necessity to develop more sophisticated stochastic theoretical models to directly connect the tumbling of the protein with the conformational states of the label performing studies of the cross correlation between the RMSD and the evolution of the dihedral angles. This theoretical methodology has to provide a univocal, consistent and general way for the interpretation of the EPR spectra of biological systems attributing a physical meaning to parameters included in it and be easy to apply by a broader community without over parameterization. Now that we elucidated experimental CW EPR spectra of the Aurora-A kinase, the effect of inhibitors and binding partners can be tested.

#### **Author contribution**

R.B., A.J.F. and M.G.C designed the research. M.G.C. designed and organized the work described in this paper, performed the spectroscopic experiments, the MD and DFT calculations, calculated the theoretical EPR spectra and analysed the data. S.G.

Burgess made the MTSL-spin labelled Aurora-A used for EPR spectroscopy. M.G.C. wrote the paper with contributions from R.B., S.G.B. and A.J.F.

## Acknowledgments

This work was supported by a studentship from Bruker Ltd. and a Cancer Research UK grant (C24461/A12772 to R.B). The authors would like to acknowledge the use of the EPSRC UK National Service for Computational Chemistry Software (NSCCS) and its staff (Dr. Alexandra Simperler and Dr. Helen Tsui for some technical advice) at Imperial College London in carrying out this work. This work is a result of many discussions within the EPR and computational communities. M. G. Concilio acknowledges Dr. A. Baldansuren and Prof. D. Collison for useful discussions about the EPR lineshape analysis; Dr. N. Burton, Prof. A. Polimeno and Dr. A. Simperler for useful feedback.

## Reference

1. M. Drescher and G. Jeschke, *EPR Spectroscopy: Application in Chemistry and Biology*, Springer, Berlin, pp. 237 (2012).
2. A. J. Hoff, *Advanced EPR: Applications in Biology and Biochemistry*, Elsevier, Amsterdam, pp. 918 (1989).
3. Z. Zhang, M. R. Fleissner, D. Tipikin, Z. Liang, J. K. Moscicki, K. Earle, W. Hubbell and J. H. Freed, *J. Phys. Chem. B* **114**, 5503 (2010).
4. B. J. Gaffney, M. Bradshaw, S. Frausto, J. H. Freed, and P. P. Borbat. *Biophysical J.* 103, 2134 (2012).
5. S. C. Drew, S. L. Leong, C. L. Pham, D. J. Tew, C. L. Masters, L. A. Miles, R. Cappai, K. J. Barnham, *J. Am. Chem. Soc.* **130**, 7766 (2008).
6. H. J. Steinhoff, *Biol. Chem.* **385**, 913 (2004).
7. D. Fasshauer, *Biochim. Biophys. Acta* **1641**, 87 (2003).
8. C. Bagn  ris, P. G. Decaen, B. A. Hall, C. E. Naylor, D. E. Clapham, C. W. Kay and B. A. Wallace, *Nat. Commun.* **4**, 2465 (2013).
9. Z. Zhang, M. R. Fleissner, D. S. Tipikin, Z. Liang, J. K. Moscicki, K. A. Earle, W. L. Hubbell, and J. H. Freed. *J. Phys. Chem. B* **114**, 5503 (2010).
10. Y. Sun, Z. Zhang, V.M. Grigoryants, W.K. Myers, J.H. Freed, C.P. Scholes, F. Liu, and K. Earle. *Biochemistry* **51**, 8530 (2012).
11. B. H. Robinson, L. J. Slutsky, F. P. Auteri, *J. Chem. Phys.* **96**, 2609 (1992).
12. H. J. Steinhoff, W. L. Hubbell, *Biophys. J.* **71**, 2201 (1996).
13. D. E. Budil, K. L. Sale, K. A. Khairy, P. G. Fajer, *J. Phys. Chem. A* **110**, 3703 (2006).
14. V. S. Oganessian, *J. Magn. Reson.* **188**, 196 (2007).
15. V. S. Oganessian. *Phys. Chem. Chem. Phys.* **13**, 4724 (2011).
16. D. Sezer, J.H. Freed, and B. Roux. *J. Phys. Chem. B* **112**, 11014 (2008).
17. D. Sezer, J. H. Freed, B. Roux, *J. Am. Chem. Soc.* **131**, 2597 (2009).
18. H. Li, M. Fajer, W. Yang, *J. Chem. Phys.* **126**, 024106 (2007).
19. M. I. Fajer, H. Li, W. Yang, P. G. Fajer, *J. Am. Chem. Soc.* **129**, 13840 (2007).
20. V. Barone and A. Polimeno, *Phys. Chem. Chem. Phys.* **8**, 4609 (2006).
21. L. Hermosilla, C. Sieiro, P. Calle, M. Zerbetto and A. Polimeno, *J. Phys. Chem. B*, **112**, 11202 (2008).
22. M. Zerbetto, A. Polimeno, V. Barone, *Comput. Phys. Commun.* **180**, 2680 (2009).
23. F. Tombolato, A. Ferrarini and J. H. Freed, *J. Phys. Chem. B* **110**, 26248 (2006).
24. F. Tombolato, A. Ferrarini and J. H. Freed, *J. Phys. Chem. B* **110**, 26260 (2006).
25. E. Stendardo, A. Pedone, P. Cimino, M. C. Menziani, O. Crescenzi and V. Barone, *Phys. Chem. Chem. Phys.* **12**, 11697 (2010).
26. V. Barone, P. Cimino and E. Stendardo, *J. Chem. Theory Comput.* **4**, 751 (2008).
27. V. Barone, and P. Cimino, *Chem. Phys. Lett.* **454**, 139 (2008).
28. D. Sezer, J. H. Freed and B. Roux, *J. Phys. Chem. B* **112**, 5755 (2008).
29. V. Barone, M. Zerbetto, A. Polimeno, *J. Comput. Chem.* **30**, 2 (2009).
30. A. Polimeno, V. Barone, and J.H. Freed. Ed. Wiley: New York, NY, Chapter 12 (2012).
31. Y. Polyhach, E. Bordignon, G. Jeschke, *Phys. Chem. Chem. Phys.* **13**, 2356 (2010).
32. M. M. Hatmal, Y. Li, B. G. Hegde, P. B. Hegde, C.C. Jao, R. Langen, et al., *Biopolymers* **97**, 35 (2012).

33. G. Hagelueken, R. Ward, J. H. Naismith, O. Schiemann, *Appl. Magn. Reson.* **42**, 377 (2012).
34. A. R. Barr and F. Gergely, *J. Cell Sci.* **120**, 2987 (2007).
35. J. R. Bischoff, L. Anderson, Y. Zhu, K. Mossie, L. Ng, B. Souza, B. Schryver, P. Flanagan, F. Clairvoyant, C. Ginther, C. S. Chan, M. Novotny, D. J. Slamon and G. D. Plowman, *EMBO J.* **17**, 3052 (1998).
36. R. Bayliss, T. Sardon, I. Vernos, E. Conti, *Mol. Cell.* **12**, 851 (2003).
37. F. C. Rowan, M. Richards, R. A. Bibby, A. Thompson and R. Bayliss, J. Blagg, *ACS Chem. Biol.* **8**, 2184 (2013).
38. C. A. Dodson, M. Kosmopoulou, M.W. Richards, B. Atrash, V. Bavetsias, J. Blagg and R. Bayliss, *Biochem. J.* **427**, 19 (2010).
39. J. A. Endicott, M. E. Noble and L. N. Johnson, *Annu. Rev. Biochem.* **81**, 587 (2012).
40. M. Huse and J. Kuriyan, *Cell.* **109**, 275 (2002).
41. S. S. Taylor and A. P. Kornev, *Trends. Biochem. Sci.* **36**, 65 (2011).
42. A. J. Fielding, M. G. Concilio, G. Heaven and M. A. Hollas, *Molecules.* **19**, 16998 (2014).
43. J. A. Maier, C. Martinez, K. Kasavajhala, L. Wickstrom, K. E. Hauser, C. J. Chem. Theory Comput. **11**, 3696 (2015).
44. D.A. Case, V. Babin, J.T. Berryman, R.M. Betz, Q. Cai, D.S. Cerutti, T.E. Cheatham, III, T.A. Darden, R.E. Duke, H. Gohlke, A.W. Goetz, S. Gusarov, N. Homeyer, P. Janowski, J. Kaus, I. Kolossváry, A. Kovalenko, T.S. Lee, S. LeGrand, T. Luchko, R. Luo, B. Madej, K.M. Merz, F. Paesani, D.R. Roe, A. Roitberg, C. Sagui, R. Salomon-Ferrer, G. Seabra, C.L. Simmerling, W. Smith, J. Swails, R.C. Walker, J. Wang, R.M. Wolf, X. Wu and P.A. Kollman (2014), AMBER 14, University of California, San Francisco.
45. D.R. Hartree, *Proc. Cambridge Phil. Soc.* **24**, 89 (1928).
46. V. Fock, *Z. Phys.* **61**, 126 (1930).
47. R. Ditchfield, W. J. Hehre and J. A. Pople, *J. Chem. Phys.* **54**, 724 (1971).
48. M. J. Frisch, G. W. Trucks, H. B. Schlegel, G. E. Scuseria, M. A. Robb, J. R. Cheeseman, G. Scalmani, V. Barone, B. Mennucci, G. A. Petersson, H. Nakatsuji, M. Caricato, X. Li, H. P. Hratchian, A. F. Izmaylov, J. Bloino, G. Zheng, J. L. Sonnenberg, M. Hada, M. Ehara, K. Toyota, R. Fukuda, J. Hasegawa, M. Ishida, T. Nakajima, Y. Honda, O. Kitao, H. Nakai, T. Vreven, J. A. Montgomery, Jr., J. E. Peralta, F. Ogliaro, M. Bearpark, J. J. Heyd, E. Brothers, K. N. Kudin, V. N. Staroverov, R. Kobayashi, J. Normand, K. Raghavachari, A. Rendell, J. C. Burant, S. S. Iyengar, J. Tomasi, M. Cossi, N. Rega, J. M. Millam, M. Klene, J. E. Knox, J. B. Cross, V. Bakken, C. Adamo, J. Jaramillo, R. Gomperts, R. E. Stratmann, O. Yazyev, A. J. Austin, R. Cammi, C. Pomelli, J. W. Ochterski, R. L. Martin, K. Morokuma, V. G. Zakrzewski, G. A. Voth, P. Salvador, J. J. Dannenberg, S. Dapprich, A. D. Daniels, Ö. Farkas, J. B. Foresman, J. V. Ortiz, J. Cioslowski, and D. J. Fox, Gaussian 09, Revision D.01, Gaussian, Inc., Wallingford CT, 2009.
49. C. I. Bayly, P. Cieplak, W. D. Cornell, P. A. Kollman *J. Phys. Chem.* **97**, 10269 (1993).
50. S. G. Burgess and R. Bayliss, *Acta Crystallogr. F. Struct. Biol. Commun.* **71**, 315 (2015).
51. G. Vriend, *J. Mol. Graph.* **8**, 52 (1990).
52. V. Wong, D. A. Case, *J. Phys. Chem. B* **112**, 6013 (2008).
53. P. Håkansson, P. O. Westlund, E. Lindahlb and O. Edholmb, *Phys. Chem. Chem. Phys.* **3**, 5311 (2001).
54. G. Jeschke, *Prog. Nucl. Mag. Res. Sp.* **72**, 42 (2013).
55. Becker O.M., MacKerell A.D. Jr., Roux B., Watanabe M. Computational Biochemistry and Biophysics. (2001) 512 pages.
56. Han K., Zhang X., Yang M. (2014) Protein Conformational Dynamics. Springer.
57. M. G. Concilio, A. J. Fielding, R. Bayliss, S. G. Burgess. (2016) *Theor. Chem. Acc.* In Press
58. A. W. Götz, M. J. Williamson, D. Xu, D. Poole, S. Le Grand and R. C. Walker. *J. Chem. Theory Comput.* **9**, 3878 (2013).
59. J. R. Cheeseman, G. W. Trucks, T. A. Keith and M. J. Frisch, *J. Chem. Phys.* **104**, 5497 (1996).
60. C. Lee, W. Yang and R.G. Parr, *Phys. Rev. B* **37**, 785 (1988).
61. A. D. Becke, *J. Chem. Phys.* **98**, 5648 (1993).
62. V. S. Oganessian, *Electron Paramag. Resonan.* **24**, 32 (2015).
63. V. Barone, P. Cimino and E. Stendardo, *J. Chem. Theory Comput.* **4**, 751 (2008).
64. V. Barone, and P. Cimino, *Chem. Phys. Lett.* **454**, 139 (2008).
65. V. Barone, J. Bloino, M. Biczysko. *Phys. Chem. Chem. Phys.* **12**, 1092 (2010).
66. DREAMSLAB, accessed on 01 October, 2015, <http://dreamslab.sns.it/?pag=downloads>.
67. Tomasi J., Mennucci B., Cammi R. (2005) *Chem. Rev.* 105:2999-3093.
68. V. Barone, A. Bencini, M. Cossi, A. Di Matteo, M. Mattesini and F. Totti, *J. Am. Chem. Soc.* **120**, 7069 (1998).
69. L. Hermosilla, J. M. García de la Vega, C. Sieiro and P. Calle, *J. Chem. Theory Comput.* **7**, 169 (2011).
70. H. J. Hogben, M. Krzystyniak, G.T.P. Charnock, P.J. Hore, I. Kuprov, *J. Magn. Reson.* **208**, 179 (2011).
71. G. Moro and J. H. Freed, *J. Chem. Phys.* **74**, 3757 (1981).
72. L. J. Edwards, D. V. Savostyanov, A. A. Nevzorov, M. Concistrè, G. Pileio, I. Kuprov, *J. Magn. Reson.* **235**, 121 (2013).
73. R. Kubo, *J. Math. Phys.* **4**, 174 (1963).
74. A. Polimeno and H. J. Freed, *J. Phys. Chem.* **99**, 10995 (1995).

75. J. H. Freed, G. V. Bruno and C. F. Polnaszek, *J. Phys. Chem.* **75**, 3385 (1971).
76. L. J. Schwartz, A. E. Stillman and J. H. Freed, *J. Chem. Phys.* **77**, 5410 (1982).
77. A. A. Nevzorov and J. H. Freed, *J. Chem. Phys.* **112**, 1413 (2000).
78. R. P. Mason, J. H. Freed, *J. Phys. Chem.* **78**, 1321 (1974).
79. A. G. Redfield, *IBM J. RES. DEV.* **1**, 19 (1957).
80. R. K. Wangsness, and F. Bloch, *Phys. Rev.* **89**, 728 (1953).
81. M. Persson, J. R. Harbridge, P. Hammarström, R. Mitri, L. Mårtensson, U. Carlsson, G. R. Eaton, S. S. Eaton. *Biophys. J.* **80**, 2886 (2001).
82. O. Burghaus, M. Rohrer, T. Gotzinger, M. Plato and K. Möbius, *Meas. Sci. Technol.* **3**, 765 (1992).
83. A. M. Popova, M. M. Hatmal, M. P. Frushicheva, E. A. Price, P. Z. Qin, I. S. Haworth. *J. Phys. Chem. B* **116**, 6387 (2012).
84. A. Ortega, D. Amoros, J. Garcia de la Torre, *Biophys. J.* **101**, 892 (2011).
85. Y. E. Nsmelov and D. D. Thomas, *Biophys Rev.* **2**, 91 (2010).
86. S. K. Misra and J. H. Freed. *Molecular Motions in Multifrequency Electron Paramagnetic Resonance*, S.K. Misra, Ed. Wiley-VCH: New York, (2011), Chapter 11.
87. Pavone, M.; Cimino, P.; Crescenzi O.; Sillanpää, A.; Barone, V. *J. Phys. Chem. B.* **111**, 8928 (2007).
88. E. Bordignon, H. Brütlich, L. Urban, K. Hideg, A. Savitsky, A. Schnegg, P. Gast, M. Engelhard, E. J. J. Groenen, K. Möbius and Heinz-Juergen Steinhoff. *Appl. Magn. Reson.* **37**, 391 (2010).

## Electronic supporting information (ESI):

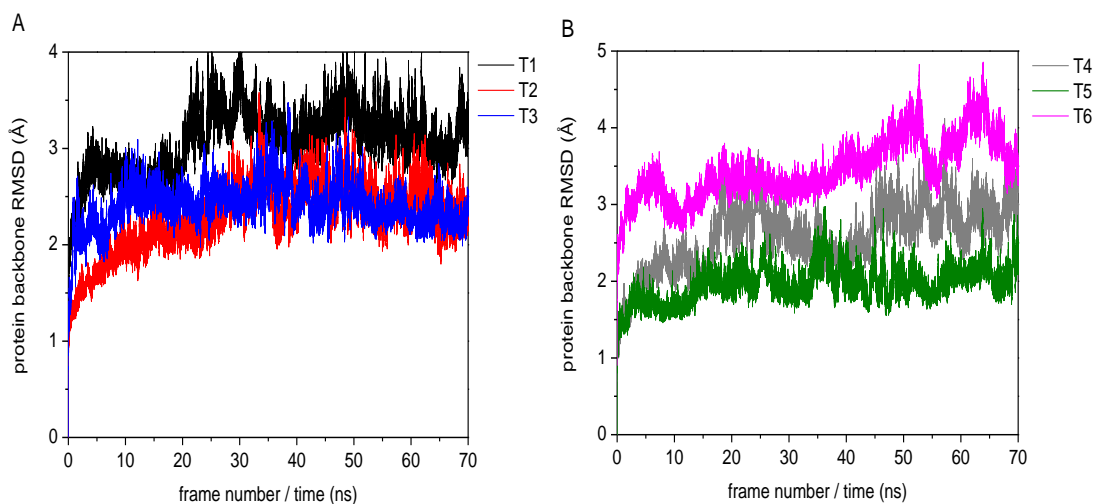


**Figure S1:** (A, B) Plots of the root mean square deviation (RMSD) of the protein backbone of T1, T2, T3, T4, T5 and T6, considering the C<sub>α</sub>, C, N, O atoms.

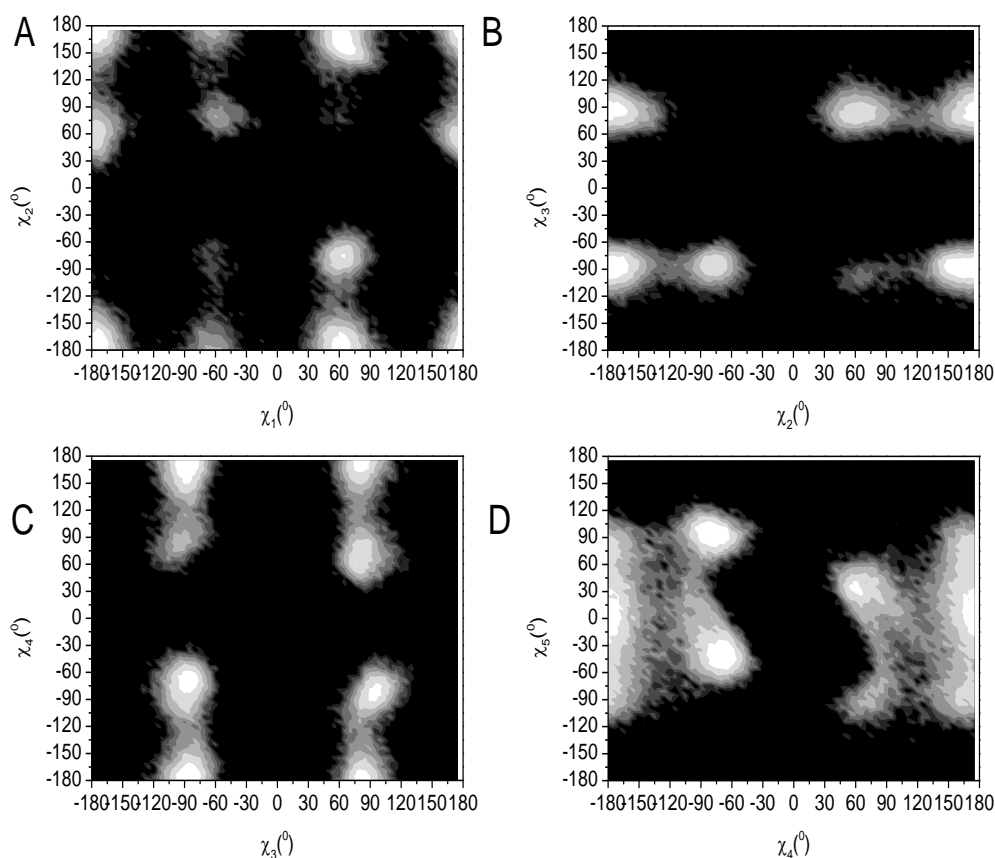


**Figure S2:** Plots of the occurrences of the  $\chi_i$ - $\chi_{i+1}$  dihedral angles for T1, (A)  $\chi_1$ - $\chi_2$ , (B)  $\chi_2$ - $\chi_3$ , (C)  $\chi_3$ - $\chi_4$  and (D)  $\chi_4$ - $\chi_5$ . The most populated regions are white and the least populated regions are black.

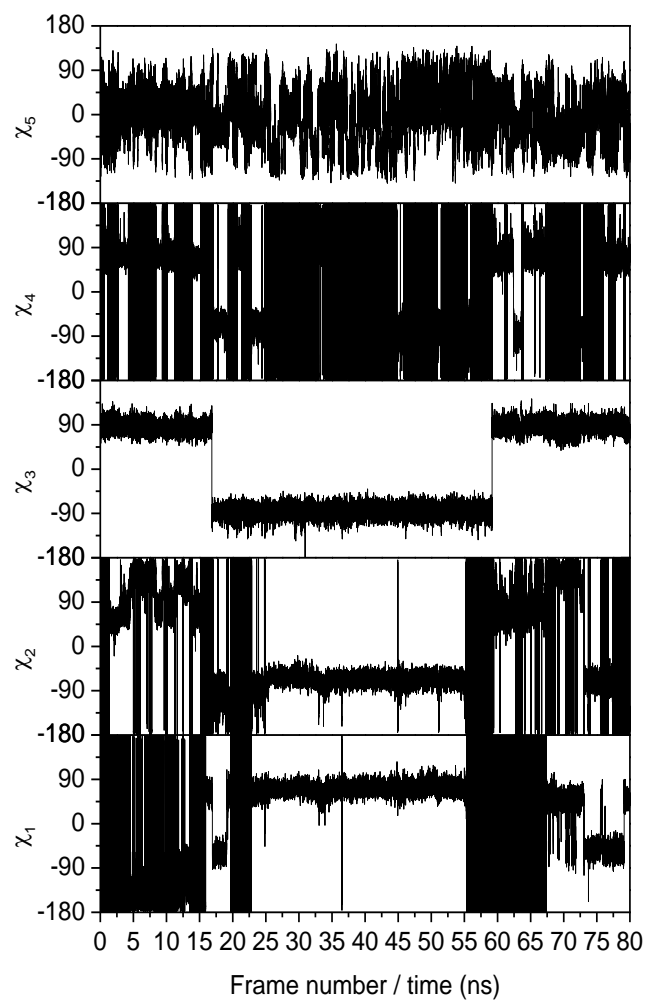


**Figure S3:** Plots showing the transitions of the  $\chi_1$  (A),  $\chi_2$  (B),  $\chi_3$  (C),  $\chi_4$  (D) and  $\chi_5$  (E) dihedral angles over 80 ns using the starting structure, T1.



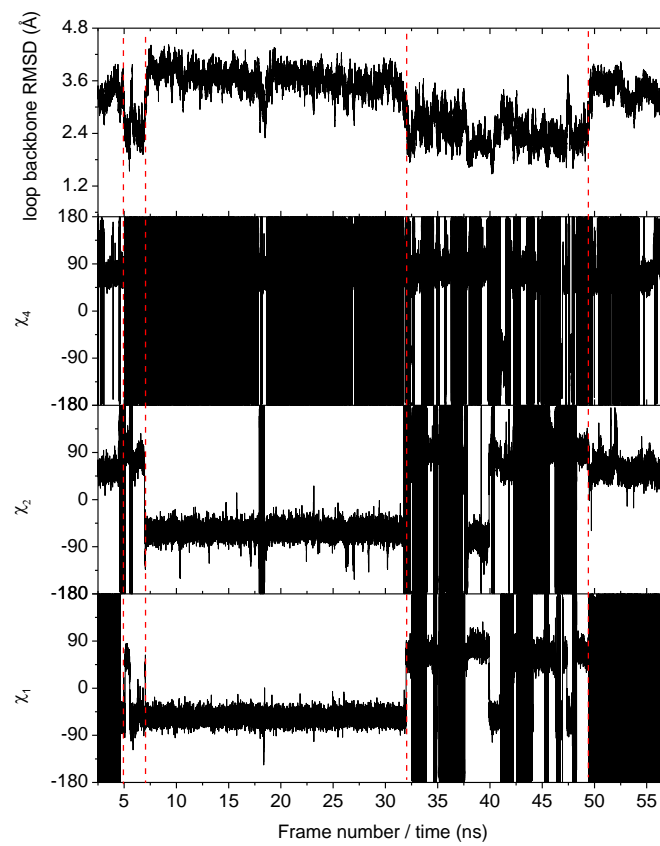


**Figure S4:** Comparison RMSD of the activation loop to the first structure after the equilibration (residues from 274 to 299, considering backbone atoms CA, C, N, O) and evolution of the  $\chi_4$  dihedral angle of the starting structure T3. The vertical dotted line indicates regions in which there are correlations between transitions of the RMSD of the activation loop and the dihedral angles.

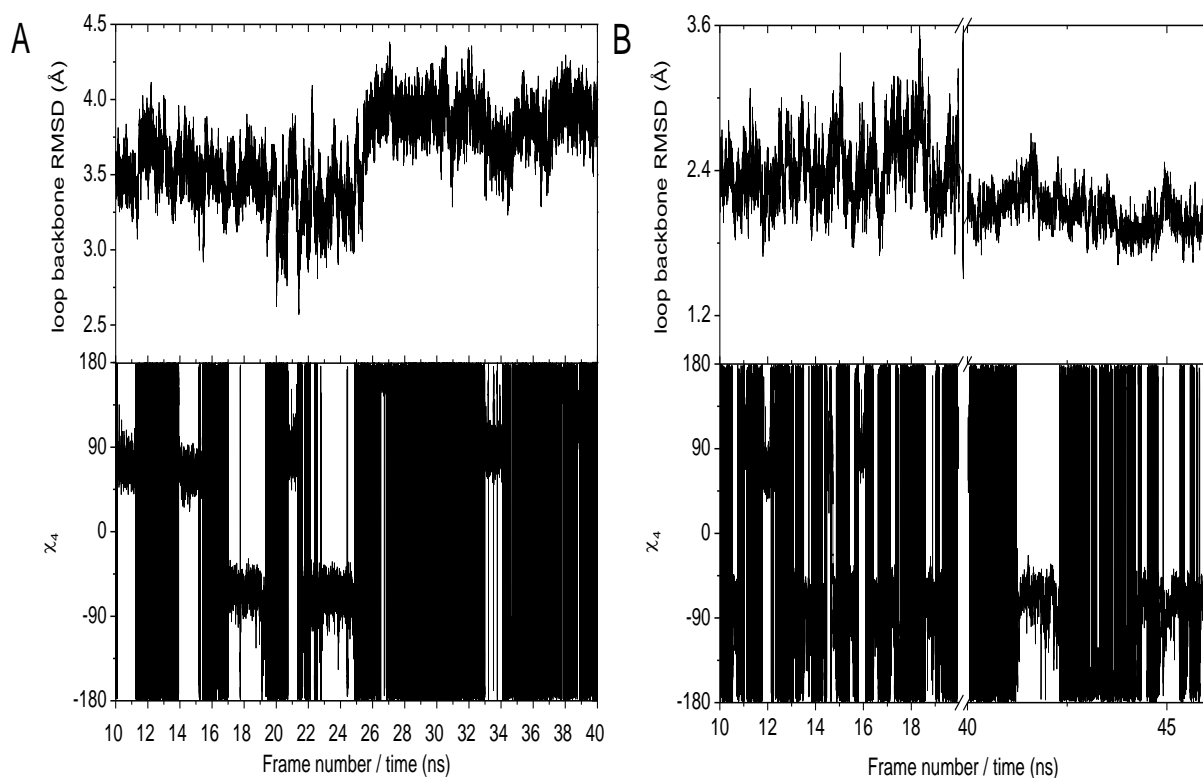


**Figure S5:** Comparison of the RMSD of the activation loop to the first structure after the equilibration (residues from 274 to 299, considering backbone atoms CA, C, N, O) and evolution of the  $\chi_4$  dihedral angle of the starting structure T1 (A) and T4 (B).

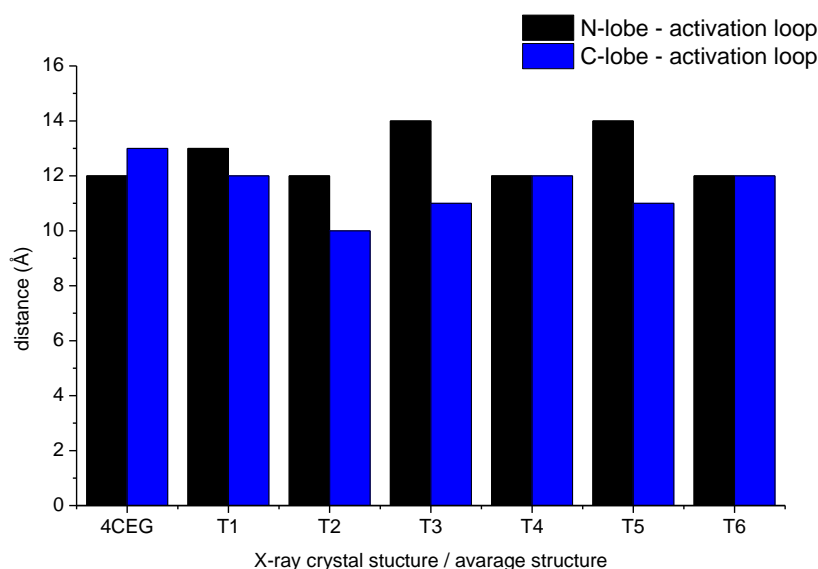


**Figure S6:** Comparison between distances between the N- and C-lobes and the activation loop observed in the average structures obtained from the MD trajectories T1, T2, T3, T4, T5, T6 and the starting X-ray crystal structure, with PDB: 4CEG. The  $C\alpha$  of the alanine 46 in the N-lobe and  $C\alpha$  of the MTSL (residue 288) in the activation loop, and the tyrosine 208 in the C-lobe and  $C\alpha$  of the MTSL were considered for the measurements.

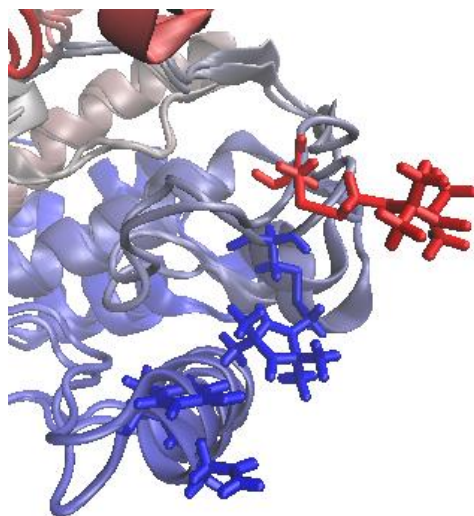


**Figure S7:** Representative average structures obtained from two MD trajectories showing the MTSL fully exposed to the solvent (red MTSL) and probing the C-lobe (blue MTSL). The remaining average structures showed similar configurations but were omitted for sake of clarity in the picture.

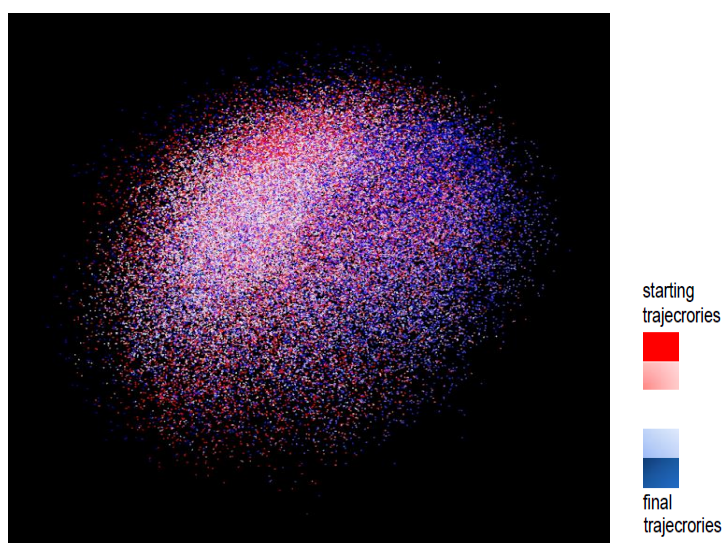


**Figure S8:** 70000 frames (70 ns) representing the isotropic and homogeneous distribution of the O atom of the MTSL NO nitroxide group in space obtained from one of the MD trajectories. Red and blue points represent the initial and final trajectories, respectively; the colour evolution is shown on the right.

**Table 1 ESI:** Evolution of the  $g_{xx}$  and  $A_{zz}$  with the polarity of the micro-environments

Structure	$A_{zz}$ (mT)	$(g_{xx}-2)\times 10^4$
<b>a</b>	3.64	84
<b>b</b>	3.64	84
<b>c</b>	3.64	85
<b>d</b>	3.48	86
<b>e</b>	2.47	87

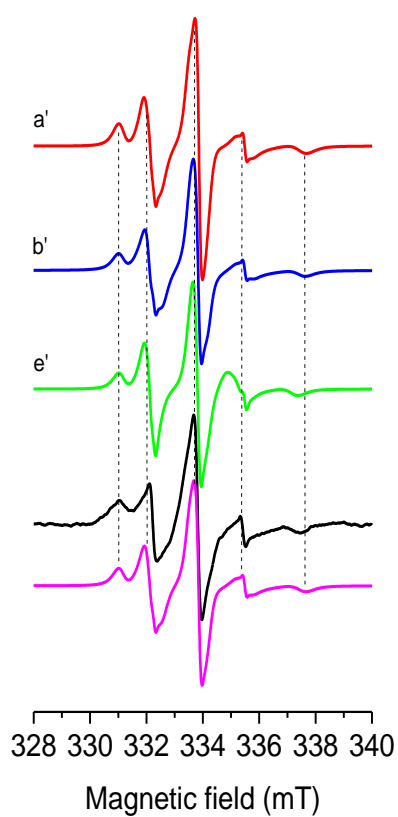


**Figure S9:** Comparison between experimental and theoretical 9 GHz EPR spectra at 298 K obtained by adding a 25% contribution of an EPR spectrum obtained using  $\tau_R$  equal to 6 ns and 14 % of the experimental spectrum of free MTSL to spectra a (a'), b (b') and e (e') in Figure 7. The black spectrum represents the experimental data and the pink spectrum represents the sum of spectra a' and b'.